Synthesis, characterization and thermal decomposition kinetics as well as evaluation of luminescent properties of several 3D lanthanide coordination polymers as selective luminescent probes of metal ions

Li-Rong Yang*, Shuang Song, Huai-Min Zhang, Lan-Zhi Wu

Institute of Molecule and Crystal Engineering, College of Chemistry and Chemical Engineering, Henan University, Kaifeng 475004, PR China

ABSTRACT

A series of 3D isomorphous and isostructural coordination polymers, namely, $\{[Ln_4(PDA)_6(H_2O)_6]\cdot H_2O\}_\infty$ (Ln = La, Nd, Sm and Gd; corresponding as-synthesized products are denoted as **1**, **2**, **3**, and **4**, respectively; PDA^{2-} = pyridine-2,6-dicarboxylate anion), were synthesized under hydrothermal conditions and characterized by means of elemental analyses, infrared spectrometry, thermal analysis and single crystal X-ray diffraction. In the meantime, the thermal decomposition kinetics of the as-synthesized complexes was investigated under non-isothermal conditions using the Achar differential method and the Coats–Redfern integral method. The room-temperature luminescent properties of the metal-organic frameworks (MOFs) of the lanthanide coordination polymers were measured. It has been found that Ln(III) centers in the complexes adopt eight-coordinated and nine-coordinated modes with N_1O_7 and N_2O_7 donors to construct distorted triangular dodecahedral and tricapped trigonal prism configurations, respectively. Based on the building block of tetranuclear homometallic $La_4C_4O_8$ unit (16-membered ring), lanthanide coordination polymers **1**–**4** are connected into highly ordered two-dimensional corrugated layers via O—C—O linkers and further assembled into 3D architectures through hydrogen bonds. Besides, lanthanide contraction effect exists in as-synthesized coordination polymers; and the lanthanide coordination polymers possess good selectivity toward metal ions such as Mg^{2+}, Cu^{2+} and Pb^{2+}, showing promising potential as selective luminescent probes of those metal ions.

© 2012 Elsevier B.V. All rights reserved.

1. Introduction

The metal-organic frameworks (MOFs) based on lanthanide-containing coordination polymers are of considerable significance owing to the combination of inorganic and organic fragments that may generate a huge number of novel architectures [1]. On the one hand, MOFs allow the manipulation of some specific functionalities based on rational design strategies for constructing porous materials with high surface areas, predictable structures, and tunable pore sizes to target some specific functionalities [2]. On the other hand, MOFs may find potentially industrial applications in gas storage and separation, catalysis, guest-exchange, molecular recognition, sensors based on optical and magnetic properties and selective luminescent probes [3]. Particularly, the highly localized f electrons of lanthanide compounds allow f–f transitions, which in association with the emission behavior of lanthanide ions within a narrow wavelength ranges results in high quantum yields. As a result, the MOFs based on lanthanide-containing coordination polymers are

intriguing and remarkably suitable for the development of optical devices and tunable luminescent sensors as well as probes for chemical species [4].

Previous researches demonstrate that efficient lanthanide luminescence in organometallic complexes is typically accomplished by the use of antenna linkers that facilitates the efficient transfer of the energy gained through photon absorption to Ln(III) ions in the complexes. This kind of recognition event can be readily transformed into an external luminescence intensity change once luminescent metal sites and/or organic linkers are incorporated into luminescent MOFs [5]. Therefore, searching for efficient antenna coordination polymers with high absorption in certain spectral regions is an attractive task. Many intriguing complexes have been reported in this respect; and it has been suggested that the Ln(III)–ligand interaction be maximized so as to increase the thermodynamic stability of the complex [6].

Naturally, hard Ln(III) ions are in favor of hard binding sites containing large electrostatic components. Therefore, anionic ligands like carboxylates are strongly recommended as the antenna linkers of Ln(III) ions, because anionic ligands may potentially provide various coordination modes and favor the construction of higher-dimensional MOFs. Specifically, pyridine-2,6-dicarboxylic

* Corresponding author.
  E-mail address: lirongyang@henu.edu.cn (L.-R. Yang).

acid (denoted as H_2PDA, as well as its deprotoned $HPDA^-$ and PDA^{2-} anions), an important carboxylate derivative possessing a rigid angle of 120° between the central pyridine ring and the two carboxyl groups, may be a promising anionic ligand for constructing porous lanthanide organic frameworks (LnOFs), because it is able to coordinate with metals through terminal monodentate, chelating, and bidentate bridging as well as through supramolecular contacts associated with hydrogen bonds and π–π interactions [7]. This means it feasible to tune the luminescent properties of LnOFs by manipulating the coordination modes of the lanthanide ions with the anionic ligands. For example, Chen et al. reported the luminescence quench of $[Eu(PDC)_{1.5}(DMF)]\cdot(DMF)_{0.5}(H_2O)_{0.5}$ in DMF (PDC = pyridine-3,5-dicarboxylate, DMF = N,N′-dimethylformamide) by Cu^{2+} coordination, possibly because the binding of pyridyl nitrogen atoms to Cu^{2+} reduced the antenna efficiency of the organic linker, PDC, thereby retarding the f–f transitions of Eu^{3+} and quenching the luminescence [8]. Zhao et al. proved that lanthanide 3d–4f heterometallic coordination polymers $\{[Ln(PDA)_3Mn_{1.5}(H_2O)_3]\cdot3.25H_2O\}_\infty$ (PDA = pyridine-2,6-dicarboxylate anion, Ln = Eu and Tb) with one dimensional channels could be potential luminescent probes of Zn^{2+}, while $\{[Dy(PDA)_3Mn_{1.5}(H_2O)_3]\cdot3.125H_2O\}_\infty$ $\{[Dy(L)_3Mn_{1.5}(H_2O)_6]\cdot8.25H_2O\}_n$ (L = 4-hydroxylpyridine-2,6-dicarboxylic acid) might serve as candidate luminescent probes of Mg^{2+} [9].

Following our ongoing efforts toward the synthesis and isolation of LnOFs [10] and hoping to validate whether as-synthesized LnOFs can be used as luminescent probes for certain metal ions, we describe here four LnOFs structures (1–4) of La(III), Nd(III), Sm(III), and Gd(III) with pyridine-2,6-dicarboxylate which form infinite 3D isomorphous and isostructural coordination polymers through the building block of $La_4C_4O_8$ unit. The structure, thermal stability and luminescent properties of as-synthesized 3D LnOFs are also reported in relation to their potentials as luminescent probes of metal ions such as Ca^{2+}, Mg^{2+}, Zn^{2+}, Cu^{2+}, Pb^{2+}, Cd^{2+} and Hg^{2+}.

2. Experimental

2.1. Reagents and general techniques

All starting chemicals are analytical grade and used without further purification. Elemental analysis was performed with a Perkin-Elmer 240C elemental analyzer. Fourier transform infrared (FT-IR) were recorded with an AVATAR 360 FT-IR spectrometer (KBr pellets, in the region of 4000–400 cm^{-1}). The crystal structure was determined with a Bruker Smart CCD X-ray single-crystal diffractometer. Fluorescent data were collected with an F-7000 FL spectrophotometer at room temperature. Thermogravimetric (TG) and differential thermogravimetric (DTG) analyses were conducted with a Perkin-Elmer TGA7 system under flowing N_2 stream (flow rate 40 mL/min) from room temperature to 1000 °C at a heating rate of 10 K/min.

2.2. Synthesis of the complexes 1–4

2.2.1. Synthesis of $\{[La_4(PDA)_6(H_2O)_6]\cdot H_2O\}_\infty$ (1)

Complex 1 was synthesized from the reaction mixture of pyridine-2,6-dicarboxylic acid and lanthanum nitrate at a molar ratio of 5:3 in 10 mL distilled water. The resultant mixture was homogenized by stirring for 20 min at ambient temperature and then transferred into 20 mL Teflon-lined stainless steel autoclave under autogenous pressure at 160 °C for 4 days and then cooled to room temperature at a rate of 5 °C/h. After filtration, the product was washed with distilled water and then dried, and colorless transparent block crystals suitable for X-ray diffraction analysis

were obtained. Elemental analysis calcd. (%) for $C_{42}H_{32}N_6O_{31}La_4$: C, 30.16; H, 1.93; N, 5.03; found: C, 29.88; H, 2.07; N, 5.11. FT-IR data (KBr pellet, cm^{-1}): 3440 (br), 1610 (s), 1588 (s), 1560 (s), 1465 (w), 1442 (s), 1395 (s), 1386 (s), 1276 (m), 1078 (w), 1015 (w), 924 (w), 830 (w), 761 (m), 730 (m), 699 (w), 659 (m), 593 (w), 520 (w), 431 (m).

2.2.2. Synthesis of $\{[Nd_4(PDA)_6(H_2O)_6]\cdot H_2O\}_\infty$ (2)

Complex 2 was synthesized by identical experimental procedures to that of 1 except that lanthanum nitrate was replaced by neodymium nitrate. Yellow block crystals suitable for X-ray diffraction analysis were finally isolated. Elemental analysis calcd. (%) for $C_{42}H_{32}N_6O_{31}Nd_4$: C, 29.78; H, 1.90; N, 4.96; found: C, 29.65; H, 1.87; N, 4.99. FT-IR data (KBr pellet, cm^{-1}): 3431 (br), 1618 (s), 1590 (s), 1568 (s), 1456 (m), 1444 (s), 1392 (s), 1374 (m), 1361 (m), 1291 (w), 1278 (w), 1177 (w), 1078 (w), 1017 (w), 926 (w), 828 (w), 761 (m), 730 (m), 695 (m), 659 (m), 583 (w), 524 (w), 473 (w), 433 (w), 413 (w).

2.2.3. Synthesis of $\{[Sm_4(PDA)_6(H_2O)_6]\cdot H_2O\}_\infty$ (3)

Complex 3 was synthesized using the same procedures for preparing 1 except that lanthanum nitrate was replaced by samarium nitrate. Yellow block crystals suitable for X-ray diffraction analysis were finally isolated. Elemental analysis calcd. (%) for $C_{42}H_{32}N_6O_{31}Sm_4$: C, 29.36; H, 1.88; N, 4.89; found: C, 29.01; H, 1.96; N, 4.81. FT-IR data (KBr pellet, cm^{-1}): 3419 (br), 1615 (s), 1592 (s), 1570 (s), 1458 (m), 1445 (s), 1394 (s), 1358 (m), 1293 (w), 1279 (w), 1176 (w), 1076 (w), 1018 (w), 927 (w), 828 (w), 760 (m), 729 (m), 694 (w), 660 (w), 584 (w), 528 (w), 468 (w), 418 (w).

2.2.4. Solvothermal Synthesis of $\{[Gd_4(PDA)_6(H_2O)_6]\cdot H_2O\}_\infty$ (4)

Complex 4 was synthesized using the same procedures for preparing 1 except that lanthanum nitrate was replaced by gadolinium nitrate. Green block crystals suitable for X-ray diffraction analysis were finally isolated. Elemental analysis calcd. (%) for $C_{42}H_{32}N_6O_{31}Gd_4$: C, 28.90; H, 1.85; N, 4.81; found: C, 28.35; H, 1.95; N, 4.86. FT-IR data (KBr pellet, cm^{-1}): 3408 (br), 1610 (s), 1590 (s), 1572 (s), 1460 (m), 1446 (s), 1385 (s), 1382 (s), 1358 (s), 1295 (w), 1280 (m), 1196 (w), 1176 (w), 1076 (m), 1019 (m), 928 (w), 828 (w), 760 (m), 730 (s), 694 (m), 661 (m), 586 (w), 529 (w), 468 (w), 436 (w).

2.3. X-ray crystallographic determination

Single-crystal X-ray diffraction measurements of complexes 1–4 were carried out on a Bruker Smart CCD X-ray single-crystal diffractometer. Reflection data were measured at 296(2) K using graphite monochromated MoKα-radiation (λ = 0.71073 Å) with ω-scan mode. All independent reflections of complexes 1–4 were collected in a range of 1.88–25.00°, 1.89–25.00°, 1.90–25.00° and 1.95–25.00°, respectively, and determined in the subsequent refinement. SADABS multi-scan empirical absorption corrections were applied to the data processing [11]. The crystal structures were solved by direct methods and Fourier synthesis. Positional and thermal parameters were refined by the full-matrix least-squares method on F^2 using the SHELXTL software package [12]. Anisotropic thermal parameters were assigned to all non-hydrogen atoms. The hydrogen atoms were set in calculated positions and refined as riding atoms with a common fixed isotropic thermal parameter. Analytical expressions of neutral-atom scattering factors were employed, and anomalous dispersion corrections were incorporated. The crystallographic data, selected bond lengths and angles for complexes 1–4 are listed in Tables 1–3, respectively.

Table 1
Summary of crystallographic data for **1–4**.

Data	1	2	3	4
CCDC deposit no.	813792	831586	831587	821039
Empirical formula	$C_{42}H_{32}N_6O_{31}La_4$	$C_{42}H_{32}N_6O_{31}Nd_4$	$C_{42}H_{32}N_6O_{31}Sm_4$	$C_{42}H_{32}N_6O_{31}Gd_4$
Formula weight	1672.38	1693.7	1718.14	1745.74
Temperature (K)	296(2)	296(2)	296(2)	296(2)
Wavelength (Å)	0.71073	0.71073	0.71073	0.71073
Crystal system	Monoclinic	Monoclinic	Monoclinic	Monoclinic
Space group	$P2(1)/c$	$P2(1)/c$	$P2(1)/c$	$P2(1)/c$
a (Å)	10.995(4)	10.9808(5)	10.9503(5)	10.9474(10)
b (Å)	17.520(7)	17.4678(7)	17.4717(8)	17.5098(16)
c (Å)	13.590(5)	13.4036(6)	13.2878(6)	13.2387(12)
α (°)	90	90	90	90
β (°)	100.308(6)	101.1770(10)	101.5260(10)	101.696(2)
γ (°)	90	90	90	90
Z	2	2	2	2
Density (calculated)	$2.156\,g\,cm^{-3}$	$2.230\,g\,cm^{-3}$	$2.291\,g\,cm^{-3}$	$2.333\,g\,cm^{-3}$
$F(000)$	1604	1628	1644	1660
Crystal size (mm^3)	$0.22 \times 0.20 \times 0.19$	$0.18 \times 0.15 \times 0.12$	$0.44 \times 0.38 \times 0.24$	$0.46 \times 0.34 \times 0.27$
Range for data collection (°)	1.88–25.00	1.89–25.00	1.90–25.00	1.95–25.00
Limiting indices	$-12 \leq h \leq 13$, $-20 \leq k \leq 16$, $-16 \leq l \leq 14$	$-13 \leq h \leq 12$, $-20 \leq k \leq 20$, $-7 \leq l \leq 15$	$-11 \leq h \leq 13$, $-20 \leq k \leq 20$, $-10 \leq l \leq 15$	$-9 \leq h \leq 13$, $-20 \leq k \leq 20$, $-15 \leq l \leq 12$
Reflections collected/unique	12,599/4519 [$R_{int} = 0.0253$]	12,744/4429 [$R_{int} = 0.0306$]	12,548/4383 [$R_{int} = 0.0187$]	11,036/4313 [$R_{int} = 0.0218$]
Refinement method	Full-matrix least-squares on F^2	Full-matrix least-squares on F^2	Full-matrix least-squares on F^2	Full-matrix least-squares on F^2
Data/restraints/parameters	4519/6/379	4429/0/379	4383/0/379	4313/0/381
Goodness-of-fit on F^2	1.023	1.112	1.097	1.083
Volume/$Å^3$	2575.6(18)	2522.19(19)	2491.0(2)	2485.0(4)
Final R indices [$I > 2s\,(I)$]	$R_1 = 0.0246$, $wR_2 = 0.0582$	$R_1 = 0.0238$, $wR_2 = 0.0560$	$R_1 = 0.0184$, $wR_2 = 0.0442$	$R_1 = 0.0240$, $wR_2 = 0.0623$
R indices (all data)	$R_1 = 0.0223$, $wR_2 = 0.0573$	$R_1 = 0.0299$, $wR_2 = 0.0575$	$R_1 = 0.0206$, $wR_2 = 0.0449$	$R_1 = 0.0256$, $wR_2 = 0.0631$
Largest diff. peak and hole (e $Å^{-3}$)	0.576 and −0.896	0.528 and −0.490	0.508 and −0.770	1.649 and −1.473

$$R = \frac{\sum \left\| |F_0| - |F_c| \right\|}{\sum |F_0|}; \quad wR = \left\{ \frac{\sum [w(F_0^2 - F_c^2)^2]}{\sum w(F_0^2)^2} \right\}^{1/2}.$$

Table 2
Selected bond lengths (Å) for **1–4**.

Bond lengths					
Complex 1[a]					
La(1)—O(12)	2.397(3)	La(1)—O(3W)	2.587(3)	La(2)—O(6)	2.587(2)
La(1)—O(8)	2.405(3)	La(1)—N(3)	2.636(3)	La(2)—O(6A)	2.602(3)
La(1)—O(4)	2.430(3)	La(2)—O(9)	2.491(2)	La(2)—O(1W)	2.628(3)
La(1)—O(11)	2.516(3)	La(2)—O(2)	2.507(2)	La(2)—N(1)	2.651(3)
La(1)—O(2W)	2.520(3)	La(2)—O(7)	2.522(3)	La(2)—N(2)	2.691(3)
La(1)—O(10)	2.557(3)	La(2)—O(3)	2.574(3)	C(1)—O(1)	1.239(4)
Complex 2[b]					
Nd(1)—O(12)	2.337(3)	Nd(1)—O(2W)	2.535(3)	Nd(2)—O(7)	2.556(3)
Nd(1)—O(5)	2.347(3)	Nd(1)—N(3)	2.571(3)	Nd(2)—O(7)#1	2.556(2)
Nd(1)—O(4)	2.378(3)	Nd(2)—O(9)	2.443(2)	Nd(2)—O(1W)	2.558(3)
Nd(1)—O(11)	2.463(3)	Nd(2)—O(2)	2.448(3)	Nd(2)—N(1)	2.584(3)
Nd(1)—O(3W)	2.481(3)	Nd(2)—O(6)	2.475(3)	Nd(2)—N(2)	2.630(3)
Nd(1)—O(10)	2.518(3)	Nd(2)—O(3)	2.530(2)	C(1)—O(1)	1.242(4)
Complex 3[c]					
Sm(1)—O(12)	2.419(2)	Sm(1)—O(6)	2.544(2)	Sm(2)—O(10)	2.431(2)
Sm(1)—O(2)	2.420(2)	Sm(1)—N(1)	2.557(2)	Sm(2)—O(3W)	2.452(2)
Sm(1)—O(7)	2.450(2)	Sm(1)—N(2)	2.591(2)	Sm(2)—O(11)	2.502(2)
Sm(1)—O(3)	2.513(2)	Sm(2)—O(9)	2.307(2)	Sm(2)—O(2W)	2.517(2)
Sm(1)—O(6)#1	2.533(2)	Sm(2)—O(8)	2.323(2)	Sm(2)—N(3)	2.541(2)
Sm(1)—O(1W)	2.535(2)	Sm(2)—O(4)	2.352(2)	C(1)—O(1)	1.244(4)
Complex 4[d]					
Gd(1)—O(4)	2.401(2)	Gd(1)—N(2)	2.543(3)	Gd(2)—O(3W)	2.441(3)
Gd(1)—O(6)	2.411(3)	Gd(1)—N(3)	2.574(3)	Gd(2)—O(3)	2.492(3)
Gd(1)—O(10)	2.434(3)	Gd(2)—O(1)	2.287(3)	Gd(2)—O(2W)	2.504(3)
Gd(1)—O(7)	2.502(3)	Gd(2)—O(9)	2.306(3)	Gd(2)—N(1)	2.516(3)
Gd(1)—O(1W)	2.517(3)	Gd(2)—O(8)	2.332(3)	Gd(1)—O(11)	2.524(2)
Gd(1)—O(11)#1	2.524(2)	Gd(2)—O(2)	2.417(3)	C(1)—O(1)	1.254(5)
Gd(1)—O(11)	2.540(3)				

[b] Symmetry transformations used to generate equivalent atoms: #1 $-x+1, -y+1, -z+1$.

[c] Symmetry transformations used to generate equivalent atoms: #1 $-x+1, -y, -z$.

[d] Symmetry transformations used to generate equivalent atoms: #1 $-x+1, -y, -z+1$.

Table 3
Selected bond angles (°) for **1–4**.

Bond angles					
Complex 1[a]					
O(12)—La(1)—O(8)	100.05(11)	O(10)—La(1)—O(3W)	130.50(8)	O(9)—La(2)—N(1)	141.48(8)
O(12)—La(1)—O(4)	86.47(11)	O(12)—La(1)—N(3)	132.97(9)	O(2)—La(2)—N(1)	61.40(8)
O(8)—La(1)—O(4)	153.38(10)	O(8)—La(1)—N(3)	77.96(9)	O(7)—La(2)—N(1)	72.64(9)
O(12)—La(1)—O(11)	163.46(10)	O(4)—La(1)—N(3)	78.81(10)	O(3)—La(2)—N(1)	60.67(8)
O(8)—La(1)—O(11)	90.56(10)	O(11)—La(1)—N(3)	61.52(8)	O(6)—La(2)—N(1)	134.04(8)
O(4)—La(1)—O(11)	89.67(10)	O(2W)—La(1)—N(3)	126.06(10)	O(1W)—La(2)—N(1)	118.43(8)
O(12)—La(1)—O(2W)	89.85(12)	O(10)—La(1)—N(3)	60.76(8)	O(9)—La(2)—N(2)	0.16(8)
O(8)—La(1)—O(2W)	133.04(10)	O(3W)—La(1)—N(3)	139.30(9)	O(2)—La(2)—N(2)	135.61(9)
O(4)—La(1)—O(2W)	72.20(11)	O(9)—La(2)—O(2)	87.49(8)	O(7)—La(2)—N(2)	60.81(8)
O(11)—La(1)—O(2W)	73.67(11)	O(9)—La(2)—O(7)	79.45(8)	O(3)—La(2)—N(2)	70.66(8)
O(12)—La(1)—O(10)	72.77(9)	O(2)—La(2)—O(7)	78.06(8)	O(6)—La(2)—N(2)	59.59(8)
O(8)—La(1)—O(10)	77.88(9)	O(9)—La(2)—O(3)	140.81(8)	O(1W)—La(2)—N(2)	125.89(8)
O(4)La(1)—O(10)	79.55(10)	La(2)—O(6)—La(2)	117.01(9)	N(1)—La(2)—N(2)	115.55(9)
O(11)—La(1)—O(10)	122.29(8)	O(6)—La(2)—O(6)	62.99(9)	O(2)—La(2)—O(3)	121.96(8)
O(2W)—La(1)—O(10)	147.67(10)	O(9)—La(2)—O(1W)	70.61(8)	O(7)—La(2)—O(3)	82.16(9)
O(12)—La(1)—O(3W)	77.59(9)	O(2)—La(2)—O(1W)	77.02(8)	O(9)—La(2)—O(6)	83.11(8)
O(8)—La(1)—O(3W)	69.30(9)	O(7)—La(2)—O(1W)	141.51(8)	O(7)—La(2)—O(6)	120.36(8)
O(4)—La(1)—O(3W)	137.18(10)	O(3)—La(2)—O(1W)	136.19(8)	O(3)—La(2)—O(6)	76.87(8)
O(11)—La(1)—O(3W)	94.62(8)	O(6)—La(2)—O(1W)	80.07(8)	O(2)—La(2)—O(6)	108.76(8)
O(2W)—La(1)—O(3W)	68.34(10)				
Complex 2[b]					
O(12)—Nd(1)—O(5)	100.63(11)	O(12)—Nd(1)—N(3)	134.50(10)	O(9)—Nd(2)—O(1W)	70.76(8)
O(12)—Nd(1)—O(4)	84.85(11)	O(5)—Nd(1)—N(3)	77.59(9)	O(2)—Nd(2)—O(1W)	73.22(8)
O(5)—Nd(1)—O(4)	152.82(10)	O(4)—Nd(1)—N(3)	79.71(10)	O(6)—Nd(2)—O(1W)	139.03(8)
O(12)—Nd(1)—O(11)	161.35(9)	O(11)—Nd(1)—N(3)	62.76(9)	O(3)—Nd(2)—O(1W)	137.17(8)
O(5)—Nd(1)—O(11)	89.57(10)	O(3W)—Nd(1)—N(3)	125.02(10)	O(7)—Nd(2)—O(1W)	81.28(8)
O(4)—Nd(1)—O(11)	93.20(10)	O(10)—Nd(1)—N(3)	62.16(9)	O(7)#1—Nd(2)—O(1W)	67.12(8)
O(12)—Nd(1)—O(3W)	89.58(11)	O(2W)—Nd(1)—N(3)	138.12(9)	O(9)—Nd(2)—N(1)	140.63(9)
O(5)—Nd(1)—O(3W)	133.28(10)	O(9)—Nd(2)—O(2)	85.16(9)	O(2)—Nd(2)—N(1)	62.67(9)
O(4)—Nd(1)—O(3W)	72.80(10)	O(9)—Nd(2)—O(6)	79.04(8)	O(6)—Nd(2)—N(1)	72.51(9)
O(11)—Nd(1)—O(3W)	72.19(10)	O(2)—Nd(2)—O(6)	77.33(9)	O(3)—Nd(2)—N(1)	61.81(9)
O(12)—Nd(1)—O(10)	72.81(9)	O(9)—Nd(2)—O(3)	140.98(9)	O(7)—Nd(2)—N(1)	134.15(9)
O(5)—Nd(1)—O(10)	78.85(9)	O(2)—Nd(2)—O(3)	124.37(8)	O(7)#1—Nd(2)—N(1)	83.27(9)
O(4)—Nd(1)—O(10)	77.44(10)	O(6)—Nd(2)—O(3)	83.30(9)	O(1W)—Nd(2)—N(1)	115.99(9)
O(11)—Nd(1)—O(10)	124.92(8)	O(9)—Nd(2)—O(7)	84.36(8)	O(9)—Nd(2)—N(2)	70.08(9)
O(3W)—Nd(1)—O(10)	146.60(10)	O(2)—Nd(2)—O(7)	154.40(9)	O(2)—Nd(2)—N(2)	135.35(9)
O(12)—Nd(1)—O(2W)	77.65(10)	O(3)—Nd(2)—O(7)	76.70(8)	O(6)—Nd(2)—N(2)	62.19(9)
O(5)—Nd(1)—O(2W)	69.08(9)	O(9)—Nd(2)—O(7)#1	130.07(8)	O(3)—Nd(2)—N(2)	70.90(9)
O(4)—Nd(1)—O(2W)	137.73(10)	O(2)—Nd(2)—O(7)#1	106.59(9)	O(7)—Nd(2)—N(2)	61.03(8)
O(11)—Nd(1)—O(2W)	91.75(9)	O(6)—Nd(2)—O(7)#1	150.47(8)	O(7)#1—Nd(2)—N(2)	117.86(9)
O(3W)—Nd(1)—O(2W)	68.94(9)	O(3)—Nd(2)—O(7)#1	70.26(8)	O(1W)—Nd(2)—N(2)	127.23(9)
O(10)—Nd(1)—O(2W)	130.90(8)	O(7)—Nd(2)—O(7)#1	64.11(10)	N(1)—Nd(2)—N(2)	116.75(10)
Complex 3[c]					
O(12)—Sm(1)—O(2)	84.05(7)	O(3)—Sm(1)—N(1)	62.30(7)	O(10)—Sm(2)—O(3W)	71.47(8)
O(12)—Sm(1)—O(7)	78.85(7)	O(6)#1—Sm(1)—N(1)	82.42(7)	O(9)—Sm(2)—O(11)	73.18(8)
O(2)—Sm(1)—O(7)	76.93(8)	O(1W)—Sm(1)—N(1)	114.95(7)	O(8)—Sm(2)—O(11)	78.91(8)
O(12)—Sm(1)—O(3)	140.98(7)	O(12)—Sm(1)—N(2)	70.17(7)	O(4)—Sm(2)—O(11)	76.68(8)
O(2)—Sm(1)—O(3)	125.57(7)	O(2)—Sm(1)—N(2)	135.18(7)	O(10)—Sm(2)—O(11)	126.18(7)
O(7)—Sm(1)—O(3)	83.84(7)	O(7)—Sm(1)—N(2)	62.81(7)	O(3W)—Sm(2)—O(11)	146.15(8)
O(12)—Sm(1)—O(6)#1	130.61(7)	O(3)—Sm(1)—N(2)	70.82(7)	O(9)—Sm(2)—O(2W)	77.47(8)
O(2)—Sm(1)—O(6)#1	105.86(7)	O(6)#1—Sm(1)—N(2)	118.83(7)	O(8)—Sm(2)—O(2W)	69.04(7)
O(7)—Sm(1)—O(6)#1	150.37(7)	O(1W)—Sm(1)—N(2)	127.91(7)	O(4)—Sm(2)—O(2W)	137.90(8)
O(3)—Sm(1)—O(6)#1	70.47(7)	O(6)—Sm(1)—N(2)	61.73(7)	O(10)—Sm(2)—O(2W)	90.39(7)
O(12)—Sm(1)—O(1W)	70.99(7)	N(1)—Sm(1)—N(2)	117.12(8)	O(3W)—Sm(2)—O(2W)	69.34(8)
O(2)—Sm(1)—O(1W)	71.71(7)	O(9)—Sm(2)—O(8)	100.78(9)	O(11)—Sm(2)—O(2W)	130.99(7)
O(7)—Sm(1)—O(1W)	138.08(7)	O(9)—Sm(2)—O(4)	84.13(9)	O(9)—Sm(2)—N(3)	135.34(8)
O(3)—Sm(1)—O(1W)	137.37(7)	O(8)—Sm(2)—O(4)	152.50(9)	O(8)—Sm(2)—N(3)	77.43(8)
O(6)#1—Sm(1)—O(1W)	67.12(7)	O(9)—Sm(2)—O(10)	159.91(8)	O(4)—Sm(2)—N(3)	80.21(9)
O(6)#1—Sm(1)—O(6)	64.47(8)	O(8)—Sm(2)—O(10)	89.45(8)	O(10)—Sm(2)—N(3)	63.58(7)
O(1W)—Sm(1)—O(6)	81.59(7)	O(4)—Sm(2)—O(10)	94.78(8)	O(3W)—Sm(2)—N(3)	124.65(9)
O(12)—Sm(1)—N(1)	140.33(7)	O(9)—Sm(2)—O(3W)	89.15(9)	O(11)—Sm(2)—N(3)	62.60(7)
O(2)—Sm(1)—N(1)	63.39(7)	O(8)—Sm(2)—O(3W)	133.71(8)	O(2W)—Sm(2)—N(3)	137.63(8)
O(7)—Sm(1)—N(1)	72.45(7)	O(4)—Sm(2)—O(3W)	72.89(9)		
Complex 4[d]					
O(4)—Gd(1)—O(6)	83.30(9)	O(1W)—Gd(1)—N(2)	114.50(9)	O(9)—Gd(2)—O(3W)	134.18(11)
O(4)—Gd(1)—O(10)	78.57(9)	O(6)—Gd(1)—N(2)	63.95(9)	O(2)—Gd(2)—O(3W)	71.43(11)
O(6)—Gd(1)—O(10)	76.74(9)	O(11)—Gd(1)—N(2)	134.27(9)	O(9)—Gd(2)—O(3)	78.87(10)
O(4)—Gd(1)—O(7)	140.95(9)	O(4)—Gd(1)—N(3)	70.16(9)	O(8)—Gd(2)—O(3)	76.25(10)
O(6)—Gd(1)—O(7)	126.38(9)	O(6)—Gd(1)—N(3)	135.13(9)	O(2)—Gd(2)—O(3)	127.32(9)
O(10)—Gd(1)—O(7)	84.23(10)	O(10)—Gd(1)—N(3)	63.24(9)	O(3W)—Gd(2)—O(3)	145.53(10)
O(4)—Gd(1)—O(1W)	71.15(9)	O(7)—Gd(1)—N(3)	70.79(9)	O(1)—Gd(2)—O(2W)	77.42(10)
O(6)—Gd(1)—O(1W)	70.71(9)	O(1W)—Gd(1)—N(3)	128.23(9)	O(8)—Gd(2)—O(2W)	138.16(10)
O(10)—Gd(1)—O(1W)	137.42(9)	O(11)#1—Gd(1)—N(3)	119.48(9)	O(2)—Gd(2)—O(2W)	89.48(10)
O(7)—Gd(1)—O(1W)	137.52(8)	O(11)—Gd(1)—N(3)	62.17(9)	O(3W)—Gd(2)—O(2W)	69.53(10)
O(4)—Gd(1)—O(11) #1	131.01(9)	N(2)—Gd(1)—N(3)	117.27(10)	O(3)—Gd(2)—O(2W)	130.81(9)

Table 3 (*Continued*)

Bond angles					
O(6)—Gd(1)—O(11) #1	105.29(9)	O(1)—Gd(2)—O(9)	100.87(12)	O(1)—Gd(2)—N(1)	135.93(10)
O(7)—Gd(1)—O(11) #1	70.69(8)	O(1)—Gd(2)—O(8)	83.78(12)	O(9)—Gd(2)—N(1)	77.17(10)
O(10)—Gd(1)—O(11)	125.38(9)	O(9)—Gd(2)—O(8)	152.13(11)	O(8)—Gd(2)—N(1)	80.53(11)
O(1W)—Gd(1)—O(11)	81.61(8)	O(1)—Gd(2)—O(2)	158.92(10)	O(2)—Gd(2)—N(1)	64.10(9)
O(4)—Gd(1)—N(2)	140.00(9)	O(9)—Gd(2)—O(2)	89.49(10)	O(3W)—Gd(2)—N(1)	124.86(11)
O(10)—Gd(1)—N(2)	72.31(9)	O(8)—Gd(2)—O(2)	95.66(10)	O(3)—Gd(2)—N(1)	63.22(10)
O(7)—Gd(1)—N(2)	62.56(9)	O(1)—Gd(2)—O(3W)	88.40(11)	O(2W)—Gd(2)—N(1)	137.13(10)

[b] Symmetry transformations used to generate equivalent atoms: #1 $-x+1, -y+1, -z+1$.
[c] Symmetry transformations used to generate equivalent atoms: #1 $-x+1, -y, -z$.
[d] Symmetry transformations used to generate equivalent atoms: #1 $-x+1, -y, -z+1$.

3. Results and discussion

3.1. The IR spectra of the complexes

Complexes **1**–**4** are insoluble in common solvents such as CH_3COCH_3, CH_3CH_2OH, CH_3CN and tetrahydrofuran (THF), but they are soluble in CH_3OH and DMF. The structures of the complexes are identified by satisfactory elemental analysis as well as FT-IR and X-ray analyses. High yield of the products indicate that the title complexes are thermodynamically stable under the reaction conditions. The FT-IR spectra of the four as-synthesized complexes are similar. The strong and broad absorption bands in the ranges of 3440–3408 cm^{-1} and 924–928 cm^{-1} in **1**–**4** are assigned to the characteristic peaks of water molecules in coordination and lattice forms [13]. The strong vibrations around 1615 cm^{-1} and in the range of 1470–1360 cm^{-1} in **1**–**4** are ascribed to asymmetric and symmetric stretching vibrations of the carboxyl group, respectively. The values of $\Delta[\nu_{as} - \nu_s]$ are about 145 and 255 cm^{-1}, which indicates that the carboxyl groups are coordinated with the metal ions via both bidentate-chelating and mono-chelating modes [14]. The sharp peaks of δ_{O-C-O} vibration in plane emerge in the range of 660–760 cm^{-1}. The absorption at about 1570 cm^{-1} is related to
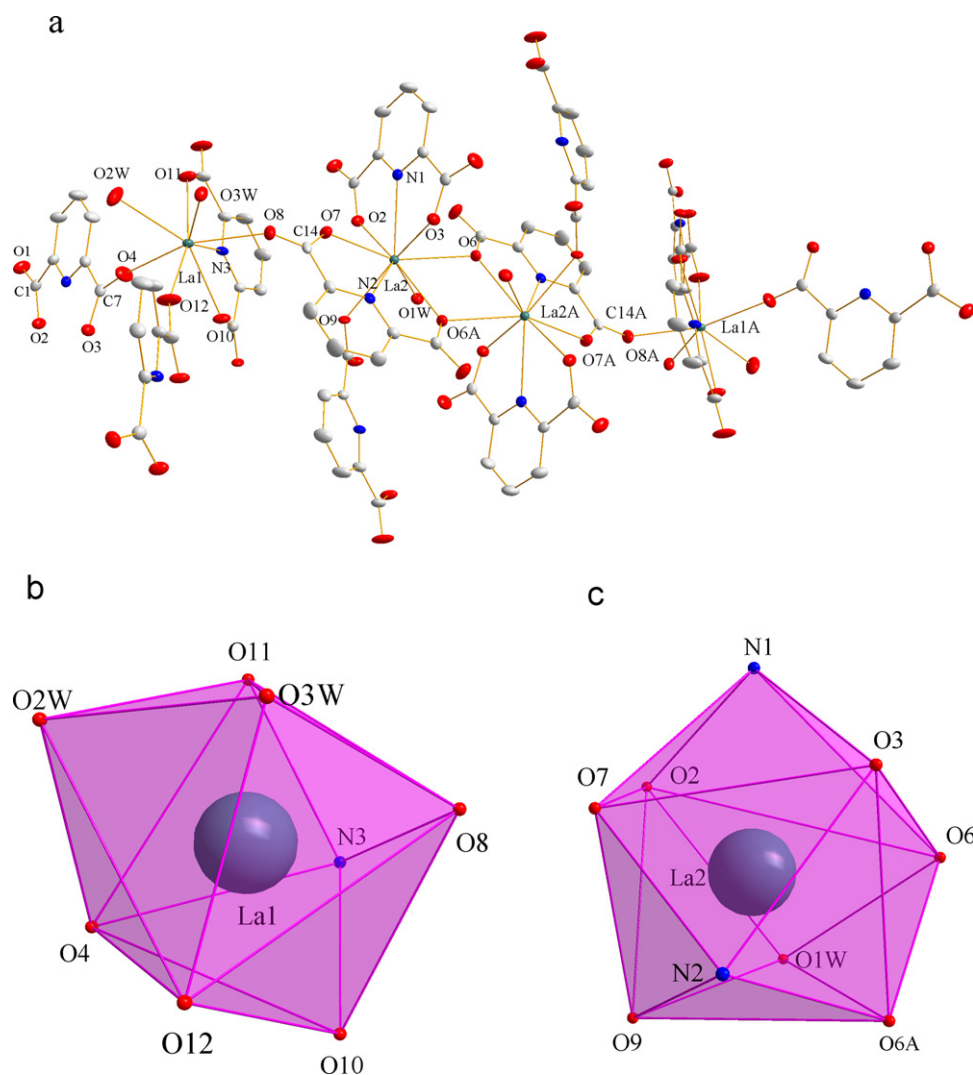

Fig. 1. (a) Coordination environment of **1** with thermal ellipsoids at 30% probability; the asymmetric unit and the related coordination atoms are labeled; lattice water and hydrogen atoms are omitted for clarity. (b and c) Highlight of the coordination polyhedra for the two crystallographically independent La(III) ions. Cyan, La; blue, N; red, O; gray, C. (For interpretation of the references to color in this figure legend, the reader is referred to the web version of the article.)

a tetradenate mode

b pentadentate mode

c pentadentate mode
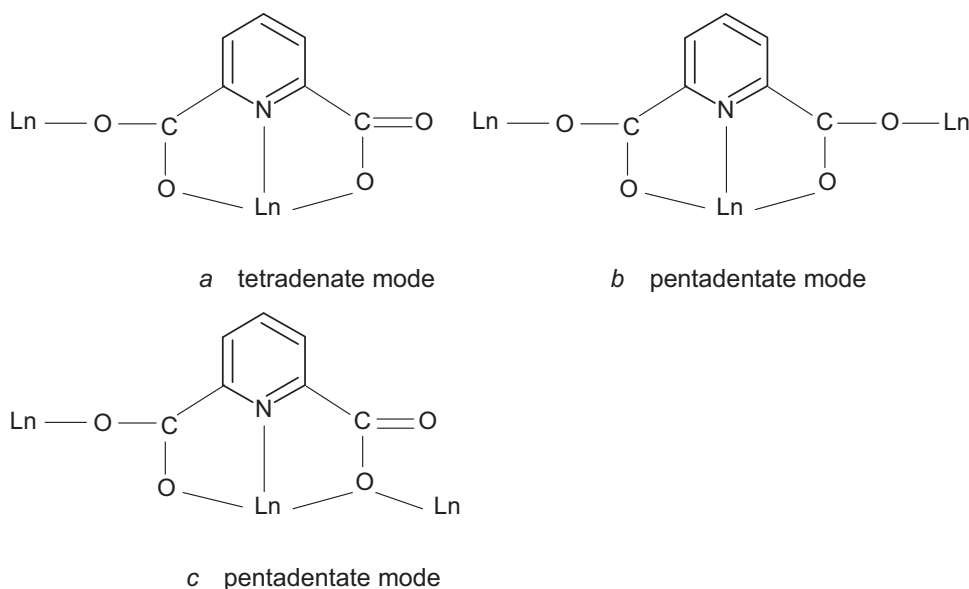
Scheme 1. Typical coordination modes of the PDA^{2-} anions in the complexes.

the NH stretching vibration [15]. The absence of the characteristic bands within 1690–1730 cm^{-1} indicates that the H$_2$PDA ligands are completely deprotonated in the form of PDA^{2-} anions upon reaction with the metal ions [16], which is also supported by the results obtained from X-ray diffraction measurements.

3.2. Structural description of the complexes

The single-crystal analyses reveal that **1**–**4** are isomorphous and isostructural, crystallizing in monoclinic space group $P2(1)/c$. Here, complex **1**, $\{[La_4(PDA)_6 (H_2O)_6]\cdot H_2O\}_\infty$, is selected as an example to describe the formation of 3D structure in detail. The coordination environment of La(III) centers in complex **1** is shown in Fig. 1 where lanthanum entities are connected with carboxylic oxygen atoms in two types of coordination environments. Namely, La(1) is eight-coordinated with the N$_1$O$_7$ donor set containing two O atoms coming from two molecules of terminal water, while La(2) is nine-coordinated with the N$_2$O$_7$ donor set containing one O atom deriving from one molecule of terminal water and the rest coordination atoms deriving from PDA^{2-} ligands. Besides, La(1) ion in the asymmetric coordination unit of **1** presents distorted triangular dodecahedral geometry, whereas La(2) ion shows tricapped trigonal prism configurations, and three kinds of coordination modes a, b and c exist in the structure (see Scheme 1). Around La(1) ion, there exist four PDA^{2-} anions: one adopts tetradentate a mode, two adopt pentadentate b mode, and one adopts pentadentate c mode; whereas four PDA^{2-} anions surround La(2) ion via one molecule of PDA^{2-} in a mode, one molecule of PDA^{2-} in b mode and two molecules in c mode. Moreover, La(1) ion is coordinated with seven O atoms and two N atoms from four PDA^{2-} anions (O(2), O(3), O(6), O(6A), O(7), O(9), N(1) and N(2)) and one terminal water molecule (O(2W) and O(3W)), while La(2) ion is coordinated with four PDA^{2-} ligands (O(4), O(8), O(10), O(11), O(12) and N(3)) and one terminal water molecule (O(1W)) to complete the coordination geometry. The La—O$_{PDA}$ distances range from 2.397(3) to 2.602(3) Å, those of La—O$_W$ are between 2.520(3) and 2.628(3) Å; and the average La—O$_{PDA}$ bond length is significantly shorter than that of La—O$_W$ bonds. The La—N distances are in the range of 2.636(3)–2.691(3) Å; and the O—La—O(N) bond angels are in the range of 59.59(8)–163.46(10)°. In addition, O(1) is not coordinated while O(2), O(3) and O(4) are coordinated with La(III) ion. As a result, C(1)—O(1) distance is shorter than that of (C(1)—O(2),

C(7)—O(3) and C(7)—O(4)), corresponding to the conjugation of the double bond after deprotonation. The bond length data in the present work are consistent with those in previous work covering lanthanide coordination polymers [17].

In the framework, La(1) and La(2) are connected through carboxylic oxygen bridges (O(7)—C(14)—O(8)) from one PDA^{2-} ligand in c mode (μ_3-(η^3-N,O,O'), O'',O''' fashion), while La(2) and La(2A) are connected through two carboxylic oxygen bridges (O(6), O(6A)) from two PDA^{2-} ligands in c mode to form an approximate rhombus La$_2$O$_2$ grid (La(2)—O(6)—La(2A)—O(6A)—La(2)). La(2)—O(6), La(2)—O(6A), La(2A)—O(6) and La(2A)—O(6A) bonds have a length of 2.587(2), 2.602(3), 2.587(2) and 2.602(4) Å, respectively, and a diagonal angles of 62.982(7)° ($\angle$O(6)—La(2)—O(6A) and O(6)—La(2A)—O(6A)) and 117.018(9)° ($\angle$La(2)—O(6)—La(2A) and $\angle$La(2)—O(6A) —La(2A)), respectively, which are close to the values reported elsewhere [10,17(a),18]. The four La(III) ions are well-separated, with the nonbonding distances of La(1)$\cdots$La(2), La(2)$\cdots$La(2A) and La(2A)$\cdots$La(1A) being 6.587(2), 4.425(1) and 6.587(2) Å, respectively, which suggests that the double-oxygen-bridge linkages of La(2)$\cdots$La(2A) is much more stronger than the O—C—O bridging linkages in La(1)$\cdots$La(2) and La(2A)$\cdots$La(1A).

The modular complex **1** is built upon the building block of tetranuclear homometallic La$_4$C$_4$O$_8$ unit (16-membered ring with the dimension of 12.448(3) × 4.425(1) Å linked through O(4), C(7), O(3), O(9A), C(15A), O(10A), O(4A), C(7A), O(3A), O(9), C(15) and
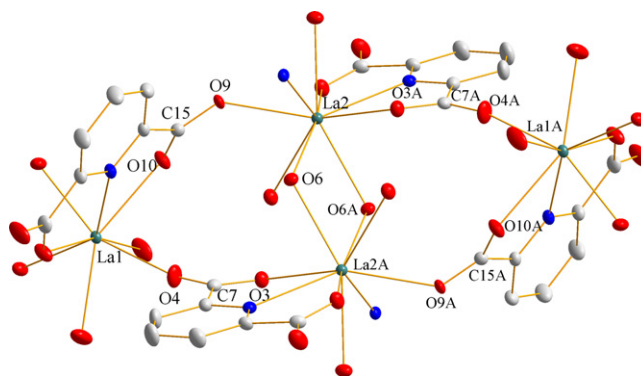

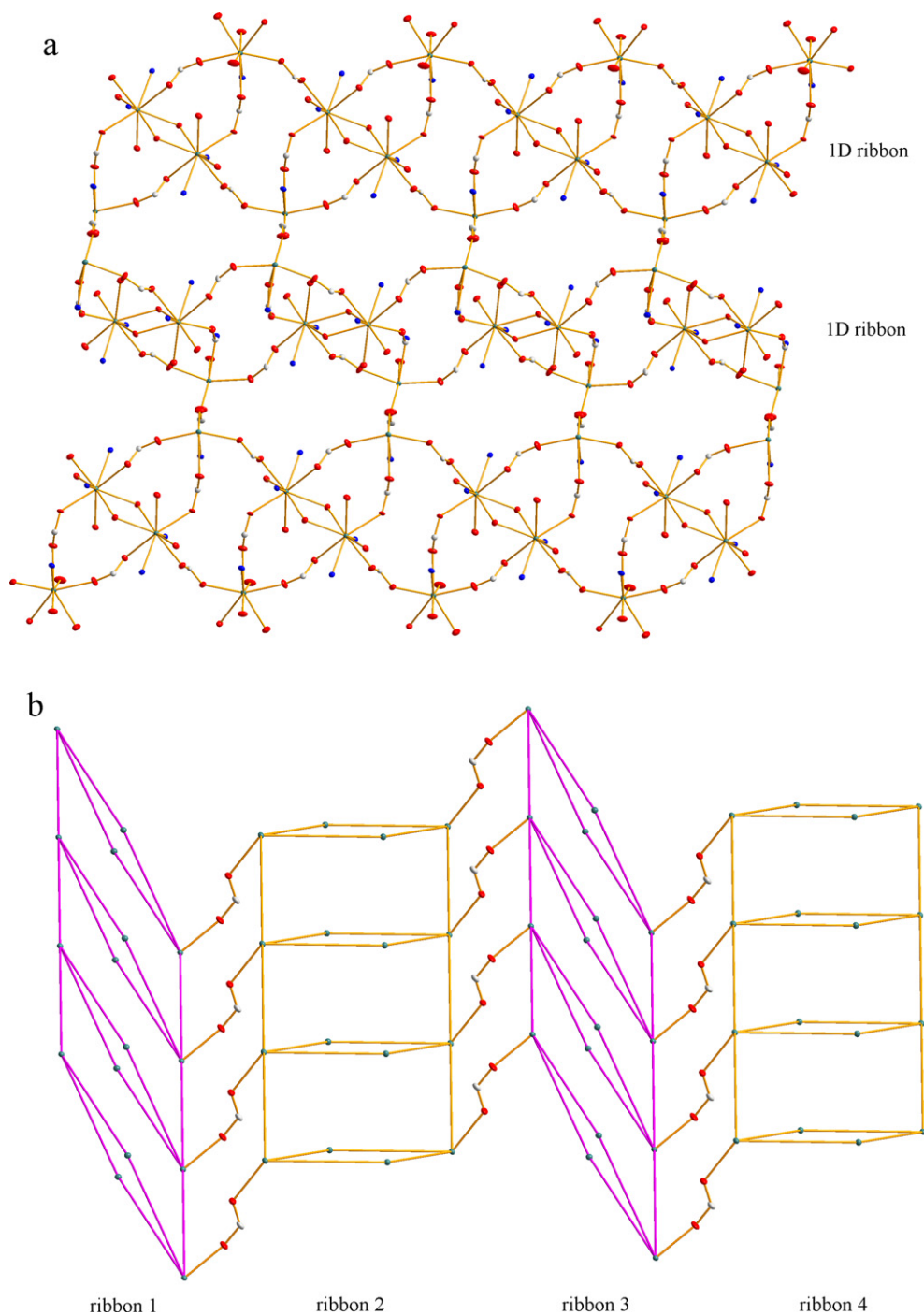**Fig. 2.** La$_4$C$_4$O$_8$ building block of complex **1**.

Fig. 3. (a) View of 2D layer generated by 1D ribbons in complex **1**; (b) view of 2D corrugated layer generated by 1D ribbons in complex **1**. Cyan, La; blue, N; red, O; gray, C. (For interpretation of the references to color in this figure legend, the reader is referred to the web version of the article.)

O(10)) whose neighboring La(III) ions are bridged by O—C—O groups in μ_2-(η^1-O),(η^1-O′) fashion and La(2) and La(2A) are bridged by O(6) and O(6A) in μ_2-(η^1-O),(η^1-O′) fashion, as illustrated in Fig. 2. The adjacent $La_4C_4O_8$ units are connected by two carboxyl bridges (O—C—O) in μ_2-(η^1-O),(η^1-O′) fashion to propagate an infinite 1D ribbon and the adjacent ribbons are connected via carboxyl bridges (O—C—O) to form a 2D corrugated layer (see Fig. 3). The 2D corrugated layer is further assembled up and down through hydrogen bonds among coordinated carboxyl oxygen atoms (O(1), O(2), O(3), O(5), O(10), O(11)) and water molecules (O(1W), O(2W), O(3W) and O(4W)) to construct a 3D polymer architecture (see Fig. 4). The parameters of hydrogen bonds are listed in Table 4. It is noteworthy that in the 2D corrugated layer, there exist two groups of

alternately arrayed parallel ribbons, namely, ribbon 1, ribbon 3,..., ribbon $2n + 1$ ($n = 0, 1, 2, 3,...$) which are reciprocally parallel with the face-to-face distance of 12.907 Å. Similarly, ribbon 2, ribbon 4,..., ribbon $2n$ ($n = 1, 2, 3,...$) are reciprocally parallel with the face-to-face distance of 8.331 Å. The dihedral angles between the two groups of ribbons are equivalent (e.g. the dihedral angle between ribbon 1 and ribbon 2 is 30.281°).

3.3. Lanthanide contraction

As above mentioned, complexes **1**–**4** are isomorphous and isostructural. In the meantime, they exhibit obvious lanthanide contraction effect, which is evidenced by their crystal lattice
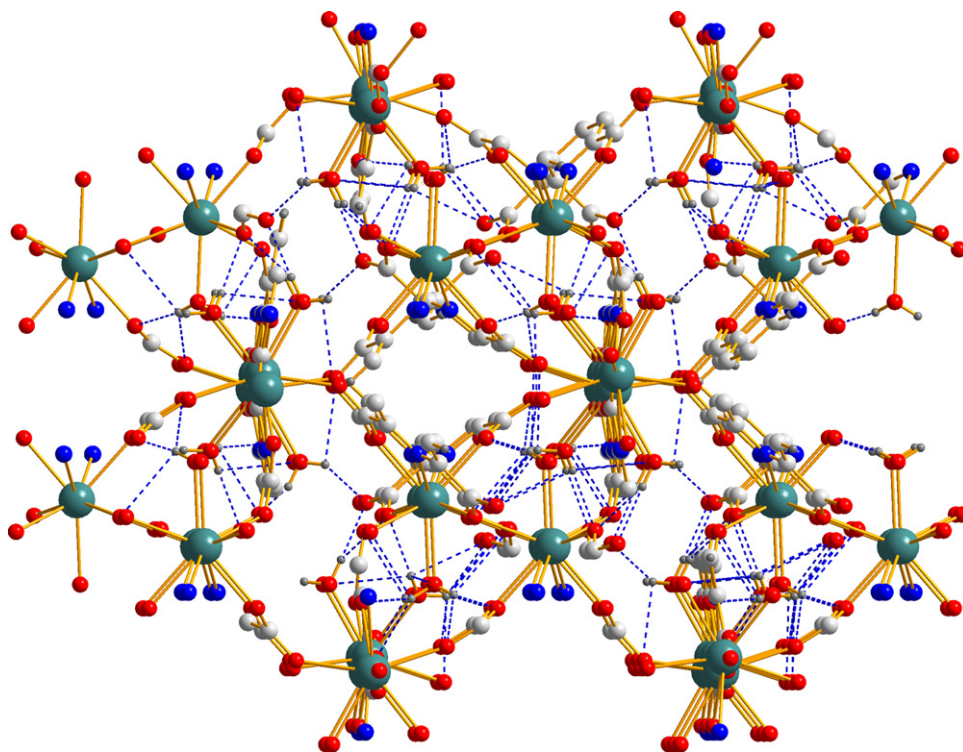
Fig. 4. Hydrogen-bonding interactions in complex **1** presenting 3D network viewed from *c*-axis direction. Cyan, La; blue, N; red, O; gray, C. (For interpretation of the references to color in this figure legend, the reader is referred to the web version of the article.)

constants. As shown in Table 5, the average distances of Ln—O_W, Ln—O_C, Ln—N and Ln···Ln in **1**–**4** decrease following an order of La, Nd, Sm and Gd, which is ascribed to the crystal field contractions of the rare earth ions lack of spherical symmetry [19]. The rare earth 4f electrons of the complexes are shielded by the $5s^2$ and $5p^6$ orbitals and hence are scarcely available for covalent interaction with the ligands. As a result, electrostatic interactions are dominant in the Ln(III) complexes, and the geometries of the complexes are determined by steric factors rather than electronic ones [5(b)]. What is noteworthy is that the bond lengths of C=O in the coordinated PDA^{2-} in **1**–**4** increase regularly with increasing in the atomic number of the lanthanide elements. For example, the bond lengths of C(1)—O(1) in **1**–**4** are 1.239(4), 1.242(4), 1.244(4) and 1.254(5) Å, respectively (see Table 2). To our knowledge, this phenomenon has not been mentioned in the literatures.

3.4. Luminescent properties

To examine the possibility of modifying the luminescent properties through cations exchange, the solid sample of **1** was immersed in CH_3OH (10^{-4} M) containing various metal cations to generate solutions at room temperature. Emission spectra of **1** in the presence of Ca^{2+}, Cd^{2+}, Mg^{2+}, Pb^{2+} and Zn^{2+} ions with respect to complex **1** are illustrated in Fig. 5. The emission intensity of complex **1** enhances gradually upon the addition of 1–3 equiv. of Mg^{2+}($Mg(CH_3COO)_2$) with respect to **1**, and its highest peak at 442 nm (excited at 392 nm) is nearly twice as intense as the corresponding peak of the solution without Mg^{2+}. Different from the above-mentioned, the introduction of Ca^{2+} ($CaCl_2$), Cd^{2+} ($Cd(CH_3COO)_2$), Pb^{2+} (10^{-3} M, $Pb(CH_3COO)_2$) and Zn^{2+} ($Zn(CH_3COO)_2$) into the CH_3OH solution of complex **1** causes only minor changes of the emission intensities.

As for **2**, when the introduction of Cu^{2+}($Cu(CH_3COO)_2$) is controlled at 2 equiv., the intensity of emission spectra at 330 and 345 nm (excited at 283 nm) reduces by 50% compared to that

without adding, while the emission intensity increases by 50% at the presence of Pb^{2+} ion (2 equiv., $Pb(CH_3COO)_2$) with respect to the original complex **1**. These emission bands are assigned to the n→π* or π→π* transition of the PDA^{2-} ligand, which suggests that the ligand-to-metal-charge-transfer (LMCT) from PDA^{2-} molecules to neodymium emission centers are moderately efficient [8,20,21]. The other metal ions including Mg^{2+}, Cd^{2+}, Hg^{2+} and Zn^{2+} do not cause so regular changes in the emission spectra of complex **2** as Cu^{2+} and Pb^{2+} ions do with respect to **2** (see Fig. 6(a) and (b)). Interestingly, the distinct decrease and enhancement of the emission intensities of **2** caused by Cu^{2+} and Pb^{2+} are more prominent at the concentration of 2 equiv. as compared with the other transition metal ions, which is related to the stronger concentration-dependent selectivity of complex **2** in the presence of Cu^{2+} and Pb^{2+} (see Fig. 6(c)).

The room-temperature luminescent spectra of **3** measured in dimethyl sulphoxide (DMSO, 10^{-4} M) are shown in Fig. 7. The broad emissions at 326 and 338 nm upon excitation at 284 nm may be due to the n→π* or π→π* transition, i.e., the ligand-to-metal-charge-transfer bands [8,20,21].

Emission spectra of **4** in the presence of Cd^{2+}, Zn^{2+} and Pb^{2+} ions with respect to original complex are depicted in Fig. 8. Only Pb^{2+}($Pb(CH_3COO)_2$) causes obvious changes in emission spectra of complex **4**. Namely, the intensity of the emission spectrum at 595 nm (excited at 458 nm) decreases with increasing Pb^{2+} concentrations (1–3 equiv.); and the emission intensity in the presence of 3 equiv. of Pb^{2+} ion is more than twice as intense as that of the corresponding band of **4** without Pb^{2+} ion. Besides, the intensity of the emission spectra at 527 nm and 685 nm (excited at 458 nm) increases upon the addition of Pb^{2+} ion; and the introduction of Cd^{2+} and Zn^{2+} causes slight decrease in the emission intensities (the other transition metal ions hardly affect the emission intensities of **4**).

The luminescent intensity of the Ln(III) relies on the efficiency of the energy transfer from the ligand to Ln(III) center [22]. Based

Table 4
Distances (Å) and angles (°) of hydrogen bonds for **1–4**.

D—H···A	d (D—H)	d (H···A)	d (D···A)	∠(D—H···A)
Complex 1[a]				
O(1W)—H(1WA)···(O3)	0.85	1.97	2.814(3)	169.1
O(1W)—H(1WB)···(O10)	0.85	2.20	2.874(4)	136.4
O(1W)—H(1WB)···(O11)	0.85	2.53	3.151(4)	131.0
O(2W)—H(2WA)···(O5)	0.85	2.34	2.873(4)	121.5
O(2W)—H(2WA)···(O4W)	0.85	2.34	2.809(14)	115.1
O(2W)—H(2WB)···(O2)	0.85	2.10	2.900(4)	157.1
O(3W)—H(3WA)···(O1)	0.85	2.10	2.849(4)	146.6
O(3W)—H(3WB)···(O1)	0.85	1.94	2.785(4)	174.2
O(4W)—H(4WA)···(O4W)	0.85	2.03	2.780(3)	117.1
Complex 2[b]				
O(4W)—H(4WA)···O(4W)#7	0.85	2.07	2.680(2)	128.0
O(3W)—H(3WA)···O(2)#8	0.85	2.53	3.008(4)	116.7
O(3W)—H(3WA)···O(1W)#8	0.85	2.25	3.076(4)	165.1
O(2W)—H(2WA)···O(1)#4	0.85	2.19	2.929(4)	145.0
O(1W)—H(1WB)···O(11)#9	0.85	2.53	3.149(4)	131.0
O(1W)—H(1WB)···O(10)#3	0.85	2.18	2.856(4)	136.8
O(3W)—H(3WB)···O(8)#10	0.85	2.47	2.925(4)	114.6
O(3W)—H(3WB)···O(4W)#10	0.85	2.05	2.855(11)	157.8
O(1W)—H(1WA)···O(3)#1	0.85	1.96	2.795(3)	167.9
O(2W)—H(2WB)···O(1)#8	0.85	1.95	2.787(4)	168.1
Complex 3[c]				
O(4W)—H(4WA)···O(4W)#7	0.85	2.25	2.839(18)	126.7
O(3W)—H(3WA)···O(2)#8	0.85	2.48	3.074(3)	127.3
O(3W)—H(3WA)···O(1W)#8	0.85	2.24	3.032(3)	155.7
O(2W)—H(2WA)···O(1)#3	0.85	2.28	2.967(3)	137.8
O(1W)—H(1WB)···O(10)#9	0.85	2.54	3.144(3)	128.5
O(1W)—H(1WB)···O(11)#4	0.85	2.15	2.848(3)	139.2
O(3W)—H(3WB)···O(5)#10	0.85	2.52	2.954(4)	112.3
O(3W)—H(3WB)···O(4W)#11	0.85	2.00	2.818(9)	161.7
O(2W)—H(2WB)···O(1)#8	0.85	1.95	2.791(3)	171.4
O(1W)—H(1WA)···O(3)#1	0.85	1.95	2.777(3)	163.9
Complex 4[d]				
O(1W)—H(1WA)···O(3)#3	0.85	2.13	2.849(4)	142.4
O(1W)—H(1WA)···O(2)#7	0.85	2.57	3.153(4)	126.8
O(1W)—H(1WB)···O(7)#1	0.85	1.95	2.770(4)	162.7
O(2W)—H(2WA)···O(5)#8	0.85	1.96	2.804(4)	170.5
O(2W)—H(2WB)···O(5)#2	0.85	2.31	3.013(4)	140.9
O(3W)—H(3WA)···O(4W)#4	0.85	1.99	2.785(12)	156.0
O(3W)—H(3WA)···O(12)#9	0.85	2.48	2.977(5)	118.1
O(3W)—H(3WB)···O(1W)#8	0.85	2.19	3.036(4)	170.8
O(4W)—H(4WB)···O(4W)#10	0.85	2.36	2.930(2)	125.5

[b] Symmetry transformations used to generate equivalent atoms: #1 −x + 1, −y + 1, −z + 1; #2 x − 1, y, z; #3 −x, −y + 1, −z + 1; #4 x, −y + 1/2, z + 1/2; #5 x + 1, y, z; #6 x, −y + 1/2, z − 1/2; #7 −x + 1, −y + 1, −z + 2; #8 −x, y − 1/2, −z + 1/2; #9 −x, y + 1/2, −z + 1/2; #10 x − 1, −y + 1/2, z − 1/2.

[c] Symmetry transformations used to generate equivalent atoms: #1 −x + 1, −y, −z; #2 x + 1, y, z; #3 x, −y + 1/2, z − 1/2; #4 −x + 2, −y, −z; #5 x − 1, y, z; #6 x, −y + 1/2, z + 1/2; #7 −x + 1, −y, −z + 1; #8 −x + 2, y + 1/2, −z + 1/2; #9 −x + 2, y − 1/2, −z + 1/2; #10 x + 1, −y + 1/2, z − 1/2.

[d] Symmetry transformations used to generate equivalent atoms: #1 −x + 1, −y, −z + 1; #2 x, −y + 1/2, z − 1/2; #3 −x + 2, −y, −z + 1; #4 x + 1, y, z; #5 x, −y + 1/2, z + 1/2; #6 x − 1, y, z; #7 −x + 2, y − 1/2, −z + 3/2; #8 −x + 2, y + 1/2, −z + 3/2; #9 x + 1, −y + 1/2, z + 1/2; #10 −x + 1, −y + 1, −z + 1.

on the results above mentioned, the emission spectra of complexes **1**, **2** and **4** change apparently upon addition of Mg^{2+}, Cu^{2+} and Pb^{2+} or Pb^{2+} ions, respectively, possibly due to relatively stronger LMCT. The energy transfer process is more effective with the introduction of certain transition metal ions [23], and LnOFs of complexes **1**, **2** and **4** may be potential ion-selective luminescent probes for Mg^{2+}, Cu^{2+} and Pb^{2+} [24]. The mechanism accounting for the luminescent feature of the complexes along with its dependence on the co-existing metal ions is still under investigation.

Table 5
Comparison of the corresponding distances (average) for complexes **1–4**.

	1 (La)	**2** (Nd)	**3** (Sm)	**4** (Gd)
Ln—O_W	2.578	2.525	2.501	2.487
Ln—O_C	2.508	2.459	2.436	2.431
Ln—N	2.659	2.595	2.563	2.544
Ln···Ln	6.587	6.521	6.485	6.476
	4.425	4.333	4.294	4.275

O_W, oxygen atom of the coordination water; O_C, oxygen atom of the carboxylate group.

3.5. Thermogravimetric analysis

Thermogravimetric analysis of **1–4** performed in the N_2 stream from room temperature to 1000 °C is particularly informative for the water content of the synthesized products, because it allows the water content present in the solvent accessible area of the 3D frameworks. As displayed in Fig. 9 and Table 6, all the LnOFs show almost similar TG curves and decompose in two steps.

The first stage weight losses of as-synthesized complexes **1–4** (7.63%, 8.61%, 8.15% and 7.97%, respectively) taking place covering the temperature ranges of 124–217, 112–210, 118–215 and 126–222 °C correspond to the destruction of one lattice water and six coordinated water molecules, which are close to relevant calculated weight loss of 7.53%, 7.44%, 7.33% and 7.22% and consistent with the crystal structure analysis. A stable plateau emerges around 210–420 °C in the TG curves, followed by the second stage weight loss at 430, 427, 429 and 440 °C owing to the ligands decomposition, giving the final residual products of Ln_2O_3. The remnants of complexes **1**, **2** and **4** at the second stage weight loss amount to 51.29% (**1**), 45.82% (**2**) and 43.82% (**4**), which suggests that they do not decompose completely under the experimental temperature

Table 6
Thermal decomposition of **1–4**.

	1	2	3	4
Dehydration temperature (°C)	124–217	112–210	118–215	126–222
Loss of water found (calcd.) (%)	7.63(7.53)	8.61(7.44)	8.15(7.33)	7.97(7.22)
Decomposition temperature (°C)	430	427	429	440
Final residual products (calcd.) (%)	51.29(38.96)	45.82(39.73)	37.68(40.59)	43.82(41.53)

(calculated values of Ln_2O_3 for complexes **1**, **2** and **4** are 38.96% (La_2O_3), 39.73% (Nd_2O_3) and 41.53% (Gd_2O_3)).

Above the second stage thermal decomposition temperature, as-synthesized lanthanide coordination polymers continue to decompose, but they do not decompose completely even at 1000 °C, showing good thermal stability. This implies that high coordination number and the coordination environment of lanthanide ions with PDA^{2-} ligand have remarkable effects on the framework rigidity and thermal stability of LnOFs **1–4**. Moreover, it is worthy to note that the dehydration and decomposition temperatures of complexes **2–4** rise with the increase of the atomic number of lanthanide elements, corresponding to the lanthanide contraction in association with the decrease of Ln—O, Ln—N and Ln···Ln distances [25].
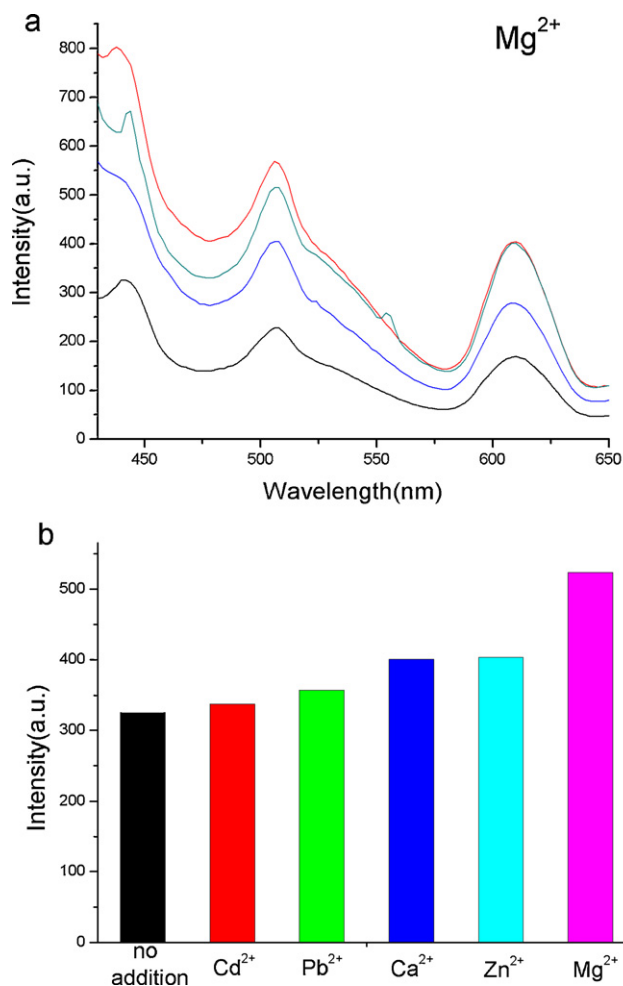

Fig. 5. (a) Emission spectra of **1** in CH_3OH (10^{-4} M) at room temperature (excited at 392 nm) in the presence of Mg^{2+} ion with respect to **1**, respectively: black, no addition; blue, 1 equiv.; green, 2 equiv.; red, 3 equiv.; (b) luminescent intensity of **1** at 442 nm in CH_3OH at room temperature upon the addition of 1 equiv. Ca^{2+}, Cd^{2+}, Mg^{2+}, Pb^{2+} and Zn^{2+} (10^{-4} M) ions (excited at 392 nm). (For interpretation of the references to color in this figure legend, the reader is referred to the web version of the article.)

3.6. Thermal decomposition kinetics studies

The TG and DTG curves of complex **1** were selected as examples to conduct the thermal decomposition kinetics studies of as-synthesized LnOFs. Relevant curves of thermal decomposition are depicted in Fig. 10. The non-isothermal kinetics of the second step was investigated using the Achar differential method and the Coats–Redfern integral method, which were conducted on the basis of 30 kinetic functions in both differential and integral forms [26]. The original kinetic data of complex **1** at the second stage of thermal decomposition, obtained from the TG and DTG curves are listed in Table 7, where T_i is the temperature at any point i on the TG and DTG curves, and α_i is the corresponding decomposition rate. $(d\alpha/dt)_i = [\beta/W_0 - W_1] \cdot (dW/dT)_i$, where $(dW/dT)_i$ is the height of the peak in the DTG curve, β is the heating rate (10 K/min), and W_0 and W_1 are the initial and final weight at the second stage of thermal decomposition. The calculated kinetic parameters (E, A) and correlation coefficients (r) of complex **1** at the second stage of thermal decomposition are listed in Table 8.

The results of thermal decomposition kinetics analysis for the second stage of thermal decomposition, obtained from the two different methods, are approximately the same when the analysis is based on No. 23 function (marked with "*" in Table 8) This function corresponds to equation $f(\alpha) = (1/4)(1 - \alpha) \cdot [-\ln(1 - \alpha)]^{-3}$, and the kinetic equation is expressed as: $d\alpha/dT = (A/\beta) \cdot \exp(-E/RT) \cdot f(\alpha)$. Further investigations show that **2–4** possess the similar kinetic equations with a general formula of $d\alpha/dT = (A/\beta) \cdot \exp(-E/RT) \cdot (1/4)(1 - \alpha) \cdot [-\ln(1 - \alpha)]^{-3}$. By substituting corresponding thermal decomposition kinetics parameters into the general formula, we have the kinetic equations of complexes **1–4** expressed as follows:

$$\frac{d\alpha}{dT} = \frac{7.88 \times 10^{77}}{\beta} \cdot (1 - \alpha)[-\ln(1 - \alpha)]^{-3} \cdot \exp\left(-\frac{1.51 \times 10^5}{T}\right),$$

$$\frac{d\alpha}{dT} = \frac{3.55 \times 10^{49}}{\beta} \cdot (1 - \alpha)[-\ln(1 - \alpha)]^{-3} \cdot \exp\left(-\frac{9.78 \times 10^4}{T}\right),$$

$$\frac{d\alpha}{dT} = \frac{2.36 \times 10^{61}}{\beta} \cdot (1 - \alpha)[-\ln(1 - \alpha)]^{-3} \cdot \exp\left(-\frac{1.19 \times 10^5}{T}\right),$$

Table 7
Data for step (2) of the thermodecomposition of the complex **1** obtained from the TG and DTG curves.

T_i (K)	W%	$d\alpha_i$	$(d\alpha/dt)_i$
782	83.8414	0.2023	0.0763
784	82.9723	0.2308	0.0831
786	82.0202	0.2620	0.0895
788	80.9881	0.2959	0.0949
790	79.871	0.3325	0.0990
792	78.6705	0.3719	0.1017
794	77.3869	0.4140	0.1025
796	76.0681	0.4572	0.1016
798	74.7354	0.5009	0.0988
800	73.4407	0.5433	0.0944
802	72.2623	0.5820	0.0885
804	71.2483	0.6152	0.0814
806	70.3772	0.6438	0.0735

Table 8
Results of the analysis of the data for step (2) in Table 6 by the differential method by ACHAR and the integral method by Coats–Redfern.

| No.	E (KJ/mol)	$\ln A$ (S^{-1})	R	E (KJ/mol)	$\ln A$ (S^{-1})	r
1	246.53	34.71	0.9202	502.43	60.89	0.9923
2	325.91	46.32	0.9587	551.07	67.74	0.9944
3	356.29	49.52	0.9676	569.69	69.12	0.9951
4	415.07	58.62	0.979	607.16	74.92	0.9963
5	175.17	21.35	0.8602	451.18	50.69	0.9906
6	591.43	85.92	0.9929	727.97	93.61	0.9986
7	171.74	24.2	0.9581	326.17	35.4	0.9975
8	61.57	7.32	0.8169	213.05	18.48	0.9974
9	6.48	−1.2	0.1603	156.48	10.02	0.9973
10	−48.61	−9.85	0.7985	99.92	1.56	0.997
11	−76.15	−14.25	0.9078	71.64	−2.67	0.9968
12	83.56	9.86	0.8018	283.14	28.05	0.9952
13	112.96	14	0.888	296.98	29.78	0.9961
14	−4.61	−3.1	0.062	244.61	22.77	0.9918
15	−130.18	−22.35	0.9078	115.71	3.71	0.9909
16	−172.04	−28.95	0.9512	72.74	−2.65	0.9897
17	−192.97	−32.33	0.9634	51.25	−5.82	0.9883
18	348.09	51.5	0.9946	425.82	50.8	0.9996
19	259.92	37.16	0.9871	77.4	−1.34	0.9871
20	−88.33	−15.88	0.8069	158.68	10.06	0.9914
21	502.27	74.31	0.9881	665.54	86.15	0.9976
22	832.79	124.14	0.9919	1004.91	136.9	0.9977
23*	1163.32	173.85	0.9932	1344.28	187.65	0.9977
24	524.44	79.49	0.9973	349.22	40.7	0.9898
25	127.65	15.99	0.914	304.09	30.59	0.9965
26	−180.96	−29.71	0.8763	180.34	13.49	0.9812
27	−357.32	−56.6	0.9432	131.18	6.23	0.9649
28	−533.67	−83.61	0.9614	94.33	0.75	0.9422
29	−38.1	−8.65	0.6368	141.89	7.21	0.9957
30	20.78	−0.12	0.3552	134.97	6.35	0.9947
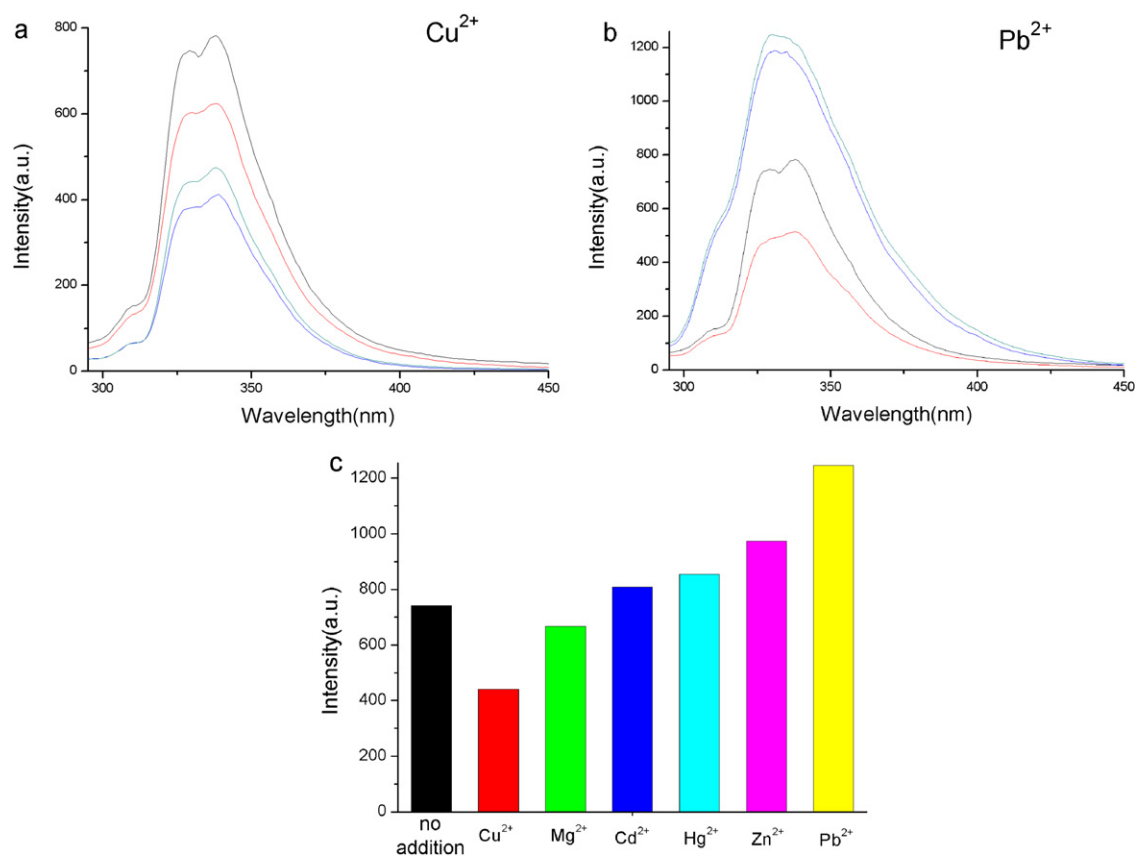
Fig. 6. (a and b) Emission spectra of **2** in DMF (10^{-4} M) at room temperature (excited at 283 nm) in the presence of 0–3 equiv. of Cu^{2+}, Mg^{2+}, Cd^{2+}, Hg^{2+}, Pb^{2+}, and Zn^{2+} ions with respect to **2**, respectively: black, no addition; red, 1 equiv.; blue, 2 equiv.; green, 3 equiv.; (c) luminescent intensity of **2** at 331 nm in DMF at room temperature upon the addition of 1 equiv. Cu^{2+}, Mg^{2+}, Cd^{2+}, Hg^{2+}, Pb^{2+}, and Zn^{2+} ions (excited at 283 nm). (For interpretation of the references to color in this figure legend, the reader is referred to the web version of the article.)
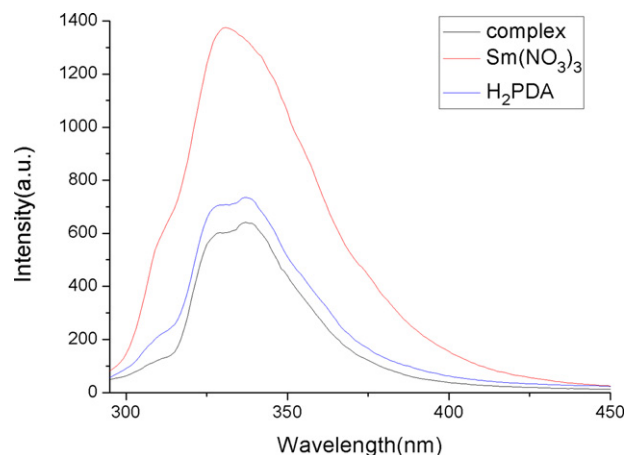
Fig. 7. Emission spectra of **3** in DMSO (10^{-4} M) at room temperature (excited at 284 nm).
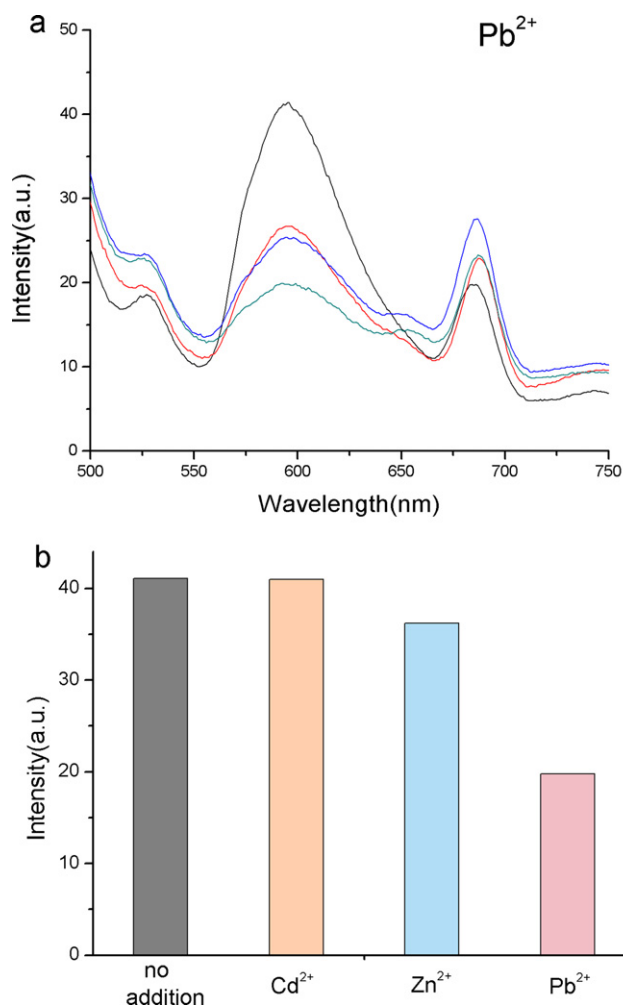

Fig. 8. (a) Emission spectra of **4** in CH_3OH (10^{-4} M) at room temperature (excited at 458 nm) in the presence of 0–3 equiv. of Pb^{2+} ions with respect to **4**, respectively: black, no addition; red, 1 equiv.; blue, 2 equiv.; green, 3 equiv.; (b) luminescent intensity of **4** at 595 nm in CH_3OH at room temperature upon the addition of 3 equiv. Cd^{2+}, Zn^{2+} and Pb^{2+} ions (excited at 458 nm). (For interpretation of the references to color in this figure legend, the reader is referred to the web version of the article.)

Table 9
Calculation values of corresponding thermodynamic parameters of **1–4**.

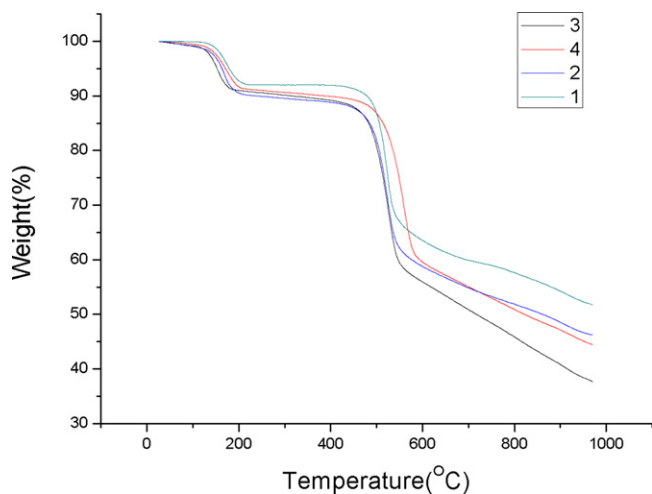| Complex	T (K)	E (KJ/mol)	$\ln A$ (S^{-1})	r	$\Delta S^{\#}$ (J/mol K)	$\Delta G^{\#}$ (KJ/mol)
1 (La)	792.96	1253.8	180.75	0.9955	1249.71	261.54
2 (Nd)	794.96	813.07	115.48	0.9994	707.01	251.70
3 (Sm)	796.97	992.79	142.70	0.9966	933.33	248.92
4 (Gd)	831.57	1068.12	147.71	0.9999	974.65	258.19

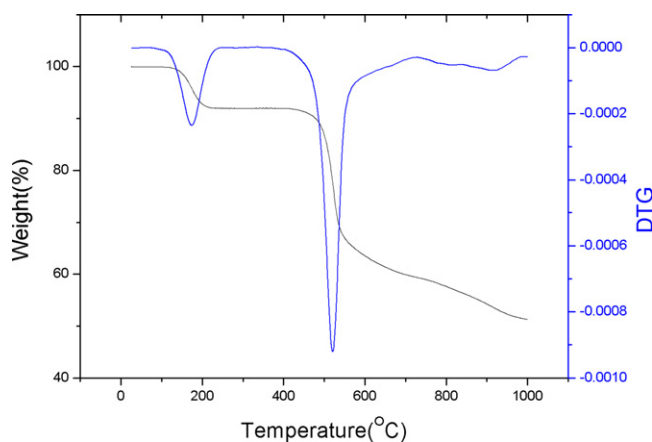**Fig. 9.** The TG curves for complexes **1**–**4**.

Fig. 10. TG and DTG curves of complex **1**.

$$\frac{d\alpha}{dT} = \frac{3.53 \times 10^{63}}{\beta} \cdot (1-\alpha)[-\ln(1-\alpha)]^{-3} \cdot \exp\left(-\frac{3.21 \times 10^5}{T}\right).$$

The activation entropy $\Delta S^{\#}$ and activation free-energy $\Delta G^{\#}$ are calculated according to the following equations: $A \exp(-E/RT) = (k_B T/h) \cdot \exp(\Delta S/R) \cdot \exp(-\Delta H/RT)$, $\Delta H = E - RT$, $\Delta G^{\neq} = \Delta H^{\neq} - T\Delta S^{\neq}$, where T is the temperature at the top of peak (2) in DTG curve, k_B is Boltzmann constant $(k_B = 1.381 \times 10^{-23} \, \text{J K}^{-1})$, R is molar gas constant $(R = 8.314 \, \text{J mol}^{-1} \, \text{K}^{-1})$, and h is Plank constant $(h = 6.626 \times 10^{-34} \, \text{J s})$ [27]. The $\Delta S^{\#}$ and $\Delta G^{\#}$ of complex **1** at the second stage of thermal decomposition are listed in Table 9.

4. Conclusion

Four novel coordination polymers containing PDA^{2-} ligand and lanthanide ion centers Ln(III) (Ln = La, Nd, Sm and Gd) with identically eight-coordinated and nine-coordinated environments and polyhedral configuration have been successfully synthesized under hydrothermal condition. As-synthesized lanthanide coordination polymers are assembled into 3D supramolecular networks based on the building blocks of homometallic La$_4$C$_4$O$_8$ unit (16-membered ring) through O—C—O bridges and hydrogen bonds. X-ray single crystal diffraction analysis indicates that complexes **1**–**4** are isomorphous and isostructural. The crystal lattice parameters, such as the average distances of Ln—O$_W$, Ln—O$_C$,

Ln—N and Ln···Ln in LnOFs **1**–**4**, regularly decrease following an order of La, Nd, Sm to Gd owing to the lanthanide contraction effect, which is also proofed by relevant thermal analysis. Besides, complexes **1**–**4** possess good thermal stability, which is closely related to the high coordination number and the coordination environment of lanthanide ions with PDA^{2-} ligand. The general formula of the thermal decomposition kinetic equation for **1**–**4** at the second stage of thermal decomposition can be expressed as: $d\alpha/dT = (A/\beta) \cdot \exp(-E/RT) \cdot 1/4(1-\alpha) \cdot [-\ln(1-\alpha)]^{-3}$. Moreover, as-synthesized LnOFs **1**, **2** and **4** possess good luminescent selectivity toward Mg^{2+}, Cu^{2+} and Pb^{2+} ions, showing promising potentials as selective luminescent probes of these metals and for the recognition of small molecules and metal ions. Further efforts will be focused on the design and assembly of lanthanide porous luminescent LnOFs with tunable micropores so as to enhance their recognition selectivity via inducing preferential binding toward different metal ions. This, hopefully, is to add to highly selective luminescent LnOFs probes for sensing metal ions.

Supplementary material

CCDC – 813792, 831586, 831587 and 821039 contain the supplementary crystallographic data for this paper. These data can be obtained free of charge via www.ccdc.cam.ac.uk/data_request/cif, or from the Cambridge Crystallographic Data Centre, 12 Union Road, Cambridge CB2 1EZ, UK. Fax: +44 1223 336 033; or e-mail: deposit@ccdc.cam.ac.uk.

Acknowledgments

References

[1] (a) T. Devic, C. Serre, N. Audebrand, J. Marrot, G. Férey, Journal of the American Chemical Society 127 (2005) 12788;
(b) G. Férey, C. Mellot-Draznieks, C. Serre, F. Millange, J. Dutour, S. Surble, I. Margiolaki, Science 309 (2005) 2040;
(c) F.N. Shi, L. Cunha-Silva, R.A.S. Ferreira, L. Mafra, T. Trindade, L. Carlos, F.A.A. Paz, J. Rocha, Journal of the American Chemical Society 130 (2008) 150.
[2] (a) A.P. Côté, A.I. Benin, N.W. Ockwig, M. O'Keeffe, A.J. Matzger, O.M. Yaghi, Science 310 (2005) 1166;
(b) O.M. Yaghi, M. O'Keeffe, N.W. Ockwig, H.K. Chae, M. Eddaoudi, J. Kim, Nature 423 (2003) 705;
(c) H.K. Chae, D.Y. Siberio-Pérez, J. Kim, Y.B. Go, M. Eddaoudi, A.J. Matzger, M. O'Keeffe, O.M. Yaghi, Nature 427 (2004) 523;
(d) B.L. Chen, M. Eddaoudi, S.T. Hyde, M. O'Keeffe, O.M. Yaghi, Science 291 (2001) 1021.
[3] (a) M. Eddaoudi, J. Kim, N. Rosi, D. Vodak, J. Wachter, M. O'Keeffe, O.M. Yaghi, Science 295 (2002) 469;
(b) M.P. Suh, Y.E. Cheon, E.Y. Lee, Coordination Chemistry Reviews 252 (2008) 1007;
(c) W.J. Rieter, K.M. Pott, K.M.L. Taylor, W. Lin, Journal of the American Chemical Society 130 (2008) 11584;
(d) M. Latroche, S. Surblé, C. Serre, C. Mellot-Draznieks, P.L. Llewellyn, J.H. Lee, J.S. Chang, S.H. Jhung, G. Férey, Angewandte Chemie International Edition 45 (2006) 8227;
(e) G.J. Halder, C.J. Kepert, B. Moubaraki, K.S. Murray, J.D. Cashion, Science 298 (2002) 1762;
(f) G. Férey, Chemical Society Reviews 37 (2007) 191;
(g) J. Guo, J. Zhang, T. Zhang, R. Wu, W. Yu, Acta Physico-Chimica Sinica 22 (2006) 1206;
(h) B.V. Harbuzaru, A. Corma, F. Rey, P. Atienzar, J.L. Jordá, H. García, D. Ananias, L.D. Carlos, J. Rocha, Angewandte Chemie International Edition 47 (2008) 1080;
(i) D.N. Dybtsev, A.L. Nuzhdin, H. Chun, K.P. Bryliakov, E.P. Talsi, V.P. Fedin, K. Kim, Angewandte Chemie International Edition 45 (2006) 916;
(j) B. Chen, L. Wang, F. Zapata, G. Qian, E.B. Lobkovsky, Journal of the American Chemical Society 130 (2008) 6718;
(k) S. Hasegawa, S. Horike, R. Matsuda, S. Furukawa, K. Mochizuki, Y. Kinoshita, S. Kitagawa, Journal of the American Chemical Society 129 (2007) 2607;
(l) S. Horike, S. Bureekaew, S. Kitagawa, Chemical Communications (2008) 471;
(m) J.H. Jia, X. Lin, C. Wilson, A.J. Blake, N.R. Champness, P. Hubberstey, G. Walker, E.J. Cussen, M. Schroder, Chemical Communications (2007) 840;

(n) B. Chen, X. Zhao, A. Putkham, K. Hong, E.B. Lobkovsky, E.J. Hurtado, A.J. Fletcher, K.M. Thomas, Journal of the American Chemical Society 130 (2008) 6411;
(o) J.P. Zhang, X.M. Chen, Journal of the American Chemical Society 130 (2008) 6010;
(p) S. Ma, X.S. Wang, D. Yuan, H.C. Zhou, Angewandte Chemie 120 (2008) 4198;
(q) M. Dincă, J.R. Long, Angewandte Chemie International Edition 120 (2008) 6870.
[4] (a) M. Kurmoo, Chemical Society Reviews 38 (2009) 1353;
(b) S. Yang, X. Lin, A.J. Blake, K.M. Thomas, P. Hubberstey, N.R. Champness, M. Schröder, Chemical Communications 46 (2008) 6108;
(c) Y.B. Dong, P. Wang, J.P. Ma, X.X. Zhao, H.Y. Wang, B. Tang, R.Q. Huang, Journal of the American Chemical Society 129 (2007) 4872;
(d) R.E. Morris, P.S. Wheatley, Angewandte Chemie International Edition 47 (2008) 4966;
(e) M. Halim, M.S. Tremblay, S. Jockusch, N.J. Turro, D. Sames, Journal of the American Chemical Society 129 (2007) 7704;
(f) M.E. Davis, Nature 417 (2002) 813;
(g) J.Y. Lee, O.K. Farha, J. Roberts, K.A. Scheidt, S.B.T. Nguyen, J.T. Hupp, Chemical Society Reviews 38 (2009) 1450;
(h) M.L. Feng, D.N. Kong, Z.L. Xie, X.Y. Huang, Angewandte Chemie International Edition 120 (2008) 8751;
(i) M. Allendorf, C. Bauer, R. Bhakta, R. Houk, Chemical Society Reviews 38 (2009) 1330;
(j) P. Wang, J.P. Ma, Y.B. Dong, R.Q. Huang, Journal of the American Chemical Society 129 (2007) 10620;
(k) J.R. Li, R.J. Kuppler, H.C. Zhou, Chemical Society Reviews 38 (2009) 1477.
[5] (a) M.D. Allendorf, C.A. Bauer, R.K. Bhakta, R.J.T. Houk, Chemical Society Reviews 38 (2009) 1330;
(b) L. Armelao, S. Quici, F. Barigelletti, G. Accorsi, G. Bottaro, M. Cavazzini, E. Tondello, Coordination Chemistry Reviews 254 (2010) 487;
(c) W.G. Lu, L. Jiang, X. Feng, T.B. Lu, Crystal Growth and Design 8 (2008) 986.
[6] (a) Q.L. Zhu, T.L. Sheng, R.B. Fu, S.M. Hu, J.S. Chen, S.C. Xiang, C.J. Shen, X.T. Wu, Crystal Growth and Design 9 (2008) 5128;
(b) T. Zhu, K. Ikarashi, T. Ishigaki, K. Uematsu, K. Toda, H. Okawa, M. Sato, Inorganica Chimica Acta 362 (2009) 3407.
[7] (a) M.G. Cai, J.D. Chen, M. Taha, Inorganic Chemistry Communications 13 (2010) 199;
(b) Z.Q. Wang, S.M. Cohen, Chemical Society Reviews 38 (2009) 1315;
(c) Y.G. Huang, D.Q. Yuan, Y.Q. Gong, F.L. Jiang, M.C. Hong, Journal of Molecular Structure 872 (2009) 99;
(d) R. Custelcean, M.G. Gorbunova, Journal of the American Chemical Society 127 (2005) 16362;
(e) T.K. Prasad, M.V. Rajasekharan, Crystal Growth and Design 6 (2006) 488;
(f) P. Mahata, K.V. Ramya, S. Natarajan, Dalton Transactions 36 (2007) 3973;
(g) J.P. Leonard, P. Jensen, T. McCabe, J.E. O'Brien, R.D. Peacock, P.E. Kruger, T. Gunnlaugsson, Journal of the American Chemical Society 129 (2007) 10986.
[8] B. Chen, L. Wang, Y. Xiao, F.R. Fronczek, M. Xue, Y. Cui, G. Qian, Angewandte Chemie International Edition 48 (2009) 500.
[9] (a) B. Zhao, X.Y. Chen, P. Cheng, D.Z. Liao, S.P. Yan, Z.H. Jiang, Journal of the American Chemical Society 126 (2004) 15394;
(b) B. Zhao, H.L. Gao, X.Y. Chen, P. Cheng, W. Shi, D.Z. Liao, S.P. Yan, Z.H. Jiang, Chemistry – A European Journal 12 (2006) 149.
[10] (a) L.R. Yang, S. Song, C.Y. Shao, W. Zhang, H.M. Zhang, Z.W. Bu, T.G. Ren, Synthetic Metals 161 (2011) 925;
(b) L.R. Yang, S. Song, C.Y. Shao, W. Zhang, H.M. Zhang, Z.W. Bu, T.G. Ren, Synthetic Metals 161 (2011) 1500;

(c) L.R. Yang, S. Song, H.M. Zhang, W. Zhang, Z.W. Bu, T.G. Ren, Synthetic Metals 161 (2011) 2230.
[11] G.M. Sheldrick, SADABS: Empirical Absorption Correction Software, University of Göttingen, Institut fur Anorganische Chemieder Universitat, Göttingen, Germany, 1999.
[12] G.M. Sheldrick, SHELXTL: Version 5. Reference Manual, Siemens Analytical X-ray Systems, USA, 1996.
[13] (a) R.R. Tang, G.L. Gu, Q. Zhao, Spectrochimica Acta Part A: Molecular and Biomolecular Spectroscopy 71 (2008) 371;
(b) K. Nakamoto, Infrared and Raman Spectra of Inorganic and Coordination Compounds, John Wiley and Sons, New York, 1997.
[14] (a) N. Tancrez, C. Feuvrie, I. Ledoux, J. Zyss, L. Toupet, H.L. Bozec, O. Maury, Journal of the American Chemical Society 127 (2005) 13474;
(b) F.N. Shi, L. Cunha-Silva, T. Trindade, F.A.A. Paz, J. Rocha, Crystal Growth and Design 9 (2009) 2098.
[15] H. Aghabozorg, A. Moghimi, F. Manteghi, M.Z. Ranjbar, Zeitschrift für Anorganische und Allgemeine Chemie 631 (2005) 909.
[16] M.S. Liu, Q.Y. Yu, Y.P. Cai, C.Y. Su, X.M. Lin, X.X. Zhou, J.W. Cai, Crystal Growth and Design 8 (2008) 4083.
[17] (a) B. Zhao, L. Yi, X.Y. Dai, X.Y. Chen, P. Cheng, D.Z. Liao, S.P. Yan, Z.H. Jiang, Inorganic Chemistry 44 (2005) 911;
(b) C. Brouca-Cabarrecq, A. Fernandes, J. Jaud, J. Costes, Inorganica Chimica Acta 332 (2002) 54;
(c) S.K. Ghosh, P.K. Bharadwaj, Inorganic Chemistry 43 (2004) 2293;
(d) H.L. Gao, L. Yi, B. Zhao, X.Q. Zhao, P. Cheng, D.Z. Liao, S.P. Yan, Inorganic Chemistry 45 (2006) 5980;
(e) Y. Song, Y. Niu, H. Hou, Y. Zhu, Journal of Molecular Structure 689 (2004) 69.
[18] S.K. Ghosh, P.K. Bharadwaj, Inorganic Chemistry 44 (2005) 3156.
[19] (a) J. Yao, B. Deng, L.J. Sherry, A.D. McFarland, D.E. Ellis, R.P. Van Duyne, J.A. Ibers, Inorganic Chemistry 43 (2004) 7735;
(b) Y.Q. Sun, G.Y. Yang, Dalton Transactions 34 (2007) 3771.
[20] C. Brouca-Cabarrecq, J. Dexpert-Ghys, A. Fernandes, J. Jaud, J.C. Trombe, Inorganica Chimica Acta 361 (2008) 2909.
[21] H. Yin, S.X. Liu, Journal of Molecular Structure 918 (2009) 165.
[22] (a) B.D. Chandler, D.T. Cramb, G.K.H. Shimizu, Journal of the American Chemical Society 128 (2006) 10403;
(b) P. Mahata, K. Ramya, S. Natarajan, Dalton Transactions (2007) 4017;
(c) N. Arnaud, E. Vaquer, J. Georges, Analyst 123 (1998) 261;
(d) T.M. Reineke, M. Eddaoudi, M. Fehr, D. Kelley, O.M. Yaghi, Journal of the American Chemical Society 121 (1999) 1651.
[23] K. Hanaoka, K. Kikuchi, H. Kojima, Y. Urano, T. Nagano, Angewandte Chemie International Edition 115 (2003) 3104.
[24] W.G. Lu, L. Jiang, X.L. Feng, T.B. Lu, Inorganic Chemistry 48 (2009) 6997.
[25] (a) C. Wang, Z. Wang, F. Gu, G. Guo, Journal of Molecular Structure 979 (2010) 92;
(b) X.F. Guo, M.L. Feng, Z.L. Xie, J.R. Li, X.Y. Huang, Dalton Transactions (2008) 3101;
(c) X.L. Chen, Y.J. Yao, H.M. Hu, S.H. Chen, F. Fu, Z.X. Han, T. Qin, M.L. Yang, G.L. Xue, Inorganica Chimica Acta 362 (2009) 2686.
[26] (a) B.N. Achar, G.W. Brindley, J.H. Sharp, Proceedings of the International Clay Conference Jerusalem 1 (1966) 67;
(b) J.H. Sharp, S.A. Wentworth, Analytical Chemistry 41 (1969) 2060;
(c) A.W. Coats, J.P. Redfern, Nature 201 (1964) 68;
(d) E. Eftimic, E. Segal, Thermochimica Acta 111 (1987) 359.
[27] R.Z. Hu, S.L. Gao, F.Q. Zhao, Q.Z. Shi, Thermal Analysis Kinetics, China 54 (2008) 116.